RESEARCH ARTICLE

Andrew J. L. Harris · William I. Rose · Luke P. Flynn

Temporal trends in lava dome extrusion at Santiaguito 1922–2000

Abstract We present a means of extracting lava dome extrusion rates from data provided by the Thematic Mapper and Enhanced Thematic Mapper Plus instruments flown on the Landsat satellites. Extrusion rates derived from the Landsat data for Santiaguito dome complex (Guatemala) during November 1987 and January 2000 of 0.72 ± 0.08 and 0.48 ± 0.09 m^3 s^{-1} compare favorably with ground-based estimates of 0.63 ± 0.28 and 0.48 ± 0.17 m^3 s^{-1}. A satellite-data-derived set of 18 extrusion rate estimates between 1987 and 2000, along with ground-based volume estimates prior to 1987, allow us to infer volumes of magma erupted since 1922. These data reveal cyclic extrusion at Santiaguito. Each cycle begins with a 3–6-year-long phase of high extrusion rate (0.5–2.1 m^3 s^{-1}), followed by a longer (3–11 years) phase of low extrusion rate (≤ 0.2 m^3 s^{-1}). The 8th cycle began in 1996 and was still in its high extrusion rate phase during January 2000. With time, however, the durations of the low extrusion rate phases have increased, peak extrusion and time-averaged extrusion rates for each cycle have decreased, and the difference between extrusion rates during the high and low extrusion rate phases of each cycle has decreased. These trends may be the result of depressurization and exhaustion of the source. In this case, the current eruption may be expected to end around 2020. Alternatively, Santiaguito may be entering a period of persistent activity maintained by a stable magma supply. In this case, we may expect extrusion to become less cyclic and to stabilize at 0.2–0.4 m^3 s^{-1}. However, a 2 wt% decrease in SiO$_2$ content of erupted products since 1970 appears to be consistent with chamber exhaustion, as well as an increase in block lava flow lengths during 1970–2000.

Introduction

The October 1902 eruption of Santa Maria (Guatemala) erupted a 8.5-km^3 volume of dense dacite and left a ~0.5-km^3 explosion crater in the southwestern flank of the previously symmetrical ~20-km^3 cone (Stoiber and Rose 1969; Williams and Self 1983). Following a 20-year period of low-level activity, characterized by geyser activity and weak ash emission (Rose 1972a), lava extrusion began during 1922 in the center of the 1902 crater (Rose 1972b) and has persisted through 2000. Extrusion rates have, however, been variable showing a distinctly cyclic pattern. Between 1922 and 1984, a dome complex, known as Santiaguito, grew in a series of 3–5-year spurts of high (0.6–2.1 m^3 s^{-1}) extrusion separated by 10–12-year intervals of lower (~0.2 m^3 s^{-1}) extrusion (Rose 1972b, 1987). By 1984, continuous slow extrusion of dacite lava had built a 0.9-km^3 complex of 22 distinct units (Rose 1987), giving an average extrusion rate of 0.46 m^3 s^{-1} for the period 1922–1984.

Extrusion continued throughout 1984–2000 (Fig. 1), and during January 2000 activity was characterized by regular (~2 h^{-1}, ≤1 km high) ash emissions from the main vent, the eruption of a block lava flow, and frequent (~1 min^{-1}) incandescent rock falls from the flow and vent area. Such activity, coupled with endogenous dome growth (Rose et al. 1970; Rose 1987), has been typical of Santiaguito since 1922. Occasional larger eruptions and dome collapses have also fed larger (~4-km-high) ash plumes and pyroclastic flow activity (e.g., SEAN 1986, 1989a). Collapse of block flow fronts caused 4-km-long Merapi-style nuée ardentes in 1973 (Rose et al. 1977), and

A.J.L. Harris (✉) · L.P. Flynn
HIGP/SOEST, University of Hawai'i, 2525 Correa Road,
Honolulu, HI 96822, USA
e-mail: Harris@pgd.hawaii.edu
Tel.: +1-808-9563157
Fax: +1-808-9566322

W.I. Rose
Department of Geological Engineering, Geology and Geophysics,
Michigan Technological University, Houghton, MI 49931, USA
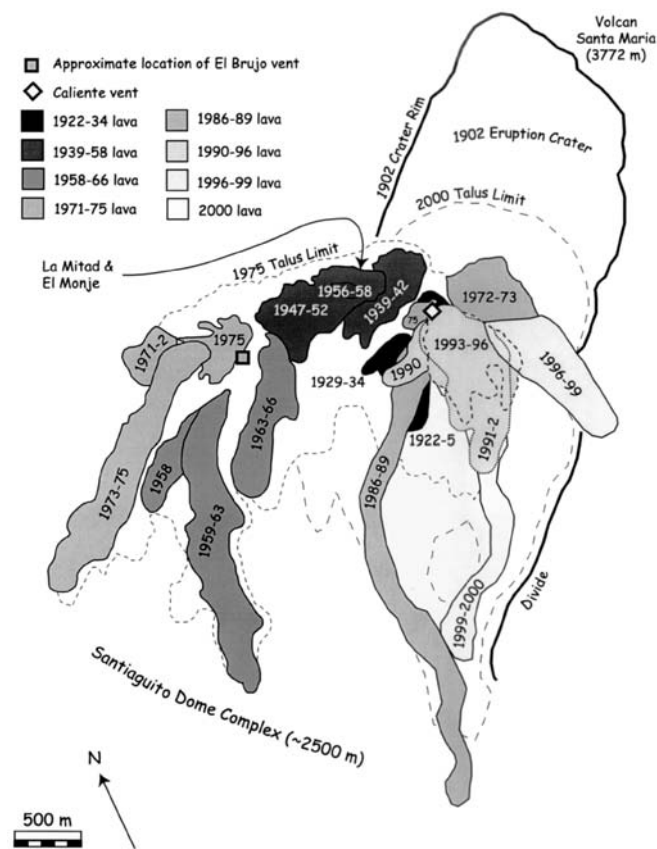
Fig. 1 Map of the individual units of the Santiaguito dome complex: 1922–1975 units are taken from Rose (1987) and 1986–2000 units are mapped using Landsat data. So that the relation of the 1993–1996, 1991–1992, and 1999–2000 units can be shown together, the proximal section of the 1999–2000 unit has not been mapped: allowing the extents of the earlier, underlying units to be seen. The 1999–2000 unit is in fact continuous all the way to the vent. For detail of the proximal section of the 1999–2000 unit, see Fig. 2

block and ash flows during 2–4 November 1929 extended ~11 km (Rose 1987).

The November 1929 block and ash flows resulted in 21 deaths at the village of El Palmar, ~10 km from Santiaguito, and the total death toll may have been as high as 5,000 (Simkin and Siebert 1994). A similar event occurring today would result in a much greater loss of life due to resettlement and increased population density (Rose 1987). Loss of life, livestock, and property also results from lahars. The inundation of El Palmar by lahars since 1983 has caused this village to be abandoned and subsequently destroyed. Defining, understanding, and tracking eruption styles and cycles at Santiaguito, therefore, is critical in assessing current and future hazard in which, for example, an increase in extrusion rate may increase the likelihood of Merapi-style pyroclastic flows and supply of volcanogenic sediment to river catchments. In this regard, Rose (1987) states that "the persistence and variety of Santiaguito's activity and the serious volcanic hazards that have been the hallmark of its history are the impetus for assembling the history of its evolution".

Regular observations of Santiaguito are made by the Santa Maria Volcano Observatory, operated by the Instituto Nacional de Sismologia, Vulcanologia, Meteorologia e Hidrologia (INSIVUMEH), located ~6.5 km south of Santiaguito. Observations are hampered, however, by frequent cloud cover and, as of January 2000, no geophysical monitoring equipment was available to the observatory staff. This coupled with the absence of direct, cloud-free lines of sight from many inhabited areas mean that chronologies to date have been based on only a few days per year of observations (Rose 1987).

This motivated our use, hence, of satellite data to obtain qualitative and quantitative data for Santiaguito and to demonstrate a remote sensing method of obtaining extrusion rate data for lava domes. This allows us to produce an activity summary for 1987–2000 and extend the 1922–1984 eruption cycle chronology of Rose (1972b, 1987) to 2000. In doing this we show that during 1987–2000 extrusion has followed the same cyclic pattern as 1922–1984, but has become concentrated at the eastern end of the dome complex.

Our data source for this study is the Thematic Mapper (TM) instrument flown on the Landsat 4 and 5 satellites and the Enhanced Thematic Mapper Plus (ETM+), which was launched on Landsat 7 during April 1999. Although the Landsat orbit allows any point on the planet to be imaged once every 16 days, the location of Santiaguito at a point where image overlap occurs means that images are available twice during every 16-day cycle, cloud permitting. Our data base consists of 29 images obtained between 1987 and 2000, of which 18 allowed cloud-free analysis of the dome complex. Obtaining cloud-free images of targets in the humid tropics can be problematic. However, despite frequent foggy conditions, the monsoonal climate at Santiaguito results in many clear mornings, especially during the dry season (November to April). As a result we find a high success rate in obtaining cloud-free morning images, the Landsat overpass time being ~10:30 a.m. (local time) and typically just before the clouds move in for the day. Obtaining cloud-free data during the wet season is much more difficult: all of our cloud-free images are from the dry season. We also note a gap in the Landsat archive for Santiaguito during March 1996 to January 2000. During this period it appears that data for this target were not recorded.

The Santiaguito eruption cycle

As defined by Rose (1972b, 1987), lava extrusion rates at Santiaguito showed a cyclic pattern between 1922 and 1984, with the dome complex growing in six spurts of extrusion. Eruptive spurts occurred in 1922–1925, 1929–1934, 1939–1942, 1949–1955, 1958–1963, and 1972–1975 (Rose 1987).

We describe below the extrusion rates and dome volumes of each of these cycles. All details and volumetric data are taken or calculated from Rose (1972b, 1987) and Rose et al. (1970), and were obtained

by the post-emplacement dimensions of each dome unit. Extrusion rates were then calculated by dividing the unit volume by the duration of emplacement. These estimates, therefore, do not include the volume of materials extruded and then moved down slope by processes such as block and ash flows and lahars. Such eroded debris enters the river catchments that drain Santiaguito, where the Landsat data define a 18.3±3.4-km^2 downstream debris fan (Harris et al. 2001). By 1979, the debris thickness was 10–15 m (Kuenzi et al. 1979), and we estimate that 30–50% of this debris (from stream bed pebble counts at a distance of ~15 km from Santiaguito) is composed of Santiaguito-derived material. This gives an eroded volume of 0.04–0.2 km^3 during 1922–1980, to which 0.01–0.03 km^3 of ash emitted during explosive events (Rose 1987) should be added. This compares with an estimated intact dome volume of 0.9 km^3 by 1980 (Rose 1987). Thus, the 1922–1980 volume may be underestimated by 5–25%, as will be any extrusion rate calculations obtained from these data.

Cycle 1: Caliente I (1922–1929)

The first dome extrusion cycle began in 1922 at the Caliente vent (Fig. 1). This vent is considered by Rose (1972b, 1987) to be the principal or central vent, being the location of strongest fumarolic and geyser activity prior to 1922 and a persistent source of gas, pyroclast, and lava emission since 1922. The initial period of high extrusion lasted until 1925, emplaced 0.2 km^3 of lava, and was accompanied by pyroclastic eruptions generating ash plumes and nuée ardentes (Rose 1972b). Peak extrusion rates of 2.06 m^3 s^{-1} were higher than during any subsequent cycle, with 22% of the 1984 dome volume being erupted during these first 3 years. The high phase was followed by a 4-year period of low (≤0.19 m^3 s^{-1}) extrusion rates until 1929. Because no lava flows were reported until 1925 (Rose 1972b), we assume that much of the growth of the dome was by endogenous processes during the high extrusion rate phase of this cycle.

Cycle 2: Caliente II (1929–1939)

The second cycle began at the Caliente vent during 1929 (Fig. 1). The initial high (0.57 m^3 s^{-1}) extrusion rate phase lasted 5 years (1929–1934) during which three ≤750-m-long block flows were extruded. This was followed by a 5-year period of low (≤0.19 m^3 s^{-1}) extrusion rates (1934–1939).

Cycle 3: La Mitad (1939–1949)

The third cycle saw activity shift ~700 m west of Caliente to become focused at La Mitad lateral vent (Fig. 1). During this cycle, a dome and flow were extruded, with the high (0.95 m^3 s^{-1}) extrusion rate phase lasting 3 years (1939–1942), followed by a 7-year-long (1942–1949) low (≤0.19 m^3 s^{-1}) extrusion rate phase. By the end of this cycle, the volume of the Santiaguito dome complex had reached 0.3 km^3.

Cycle 4: El Monje (1949–1958)

The initial high (1.24 m^3 s^{-1}) extrusion rate phase of the fourth cycle built El Monje dome and emplaced a block flow. The initial phase lasted 6 years (1949–1955), increasing the volume of the complex to 0.5 km^3. The low (≤0.19 m^3 s^{-1}) extrusion rate phase lasted 3 years (1955–1958) and built a second El Monje dome unit (Fig. 1).

Cycle 5: El Brujo (1958–1972)

The fifth cycle saw a further shift to the west, with the establishment of the El Brujo lateral vent ~1.5 km west of Caliente (Fig. 1). The high (1.49 m^3 s^{-1}) and low (≤0.57 m^3 s^{-1}) extrusion rate phases lasted 5 years (1958–1963) and 9 years (1963–1972), respectively. Extrusion rates were as low as 0.03–0.13 m^3 s^{-1} during 1967–1971. During the first phase, two block flows, 1,150 and 2,300 m long, were extruded and a third 1,200-m-long flow was extruded during the second phase (Fig. 1). Rose (1987) notes that the extrusion of these three large flows heralded a new trend, in that block flow activity increased in significance following this cycle. During the low extrusion rate phase, extrusion also occurred at Caliente where a series of plug domes were extruded at a rate of 0.13–0.16 m^3 s^{-1} during 1968–1972, with the total volume of the Santiaguito complex reaching 0.7 km^3.

Cycle 6: El Brujo and Caliente III (1972–1986)

For 3 years (1972–1975) extrusion occurred at high (0.95 m^3 s^{-1}) rates from both El Brujo and Caliente, with a 2,150-m-long block flow erupted from El Brujo (Fig. 1). During the following 11-year-long (1975–1986) low (0.25 m^3 s^{-1}) extrusion rate phase activity ceased at El Brujo (~1977). After 1975, activity continued at Caliente with the emplacement of a short (~400-m-long) block flow and repeated vertical ash eruptions becoming a prominent style of activity.

Landsat-based summary of activity: 1986–2000

Active lavas are apparent in Landsat data by virtue of their thermal signal in the 30-m-pixel shortwave infrared and the 120-m-pixel (60-m-pixels for ETM+) thermal infrared bands (e.g., Flynn et al. 1994; Andres and Rose 1995; Wooster et al. 2000). By warping these data to a contour map of the Santiaguito complex, these data have

allowed us to map the extent of block lava flow activity during 1986–2000 (Figs. 1, 2, and 3).

Our maps show that during 1986–2000 activity remained concentrated at the Caliente vent, adding further volume to this dome unit mostly by the extrusion of block flows onto the flanks of the edifice. They also reveal three further phases of activity on the basis of flow extent, in which two phases characterized by flows >1.5 km long, during 1986–1989 and 1997–2000, are separated by a period of shorter (<1.5-km-long) flows during 1990–1997. The concentration of activity at Caliente, plus the extension of two long block flows during 1986–1989 and 1999–2000, has also resulted in an increase in the zone inundated by talus (Fig. 1). In the following chronology, although we continue the naming convention used in the summary given above where eruption cycles are named after their vent location, we also distinguish between the low and high extrusion rate periods of each cycle. To do this we use postscripts a and b to denote high and low extrusion rate periods of a particular cycle, respectively.

Caliente IVa (1986–1989)

Between 1976 and 1986, extrusion from Caliente fed a block flow that extended a few hundred meters from the vent, with the oversteepened flow front generating incandescent avalanches and small block and ash flows (SEAN 1988a). During June 1986, a longer block flow began to descend the southern flank of the Caliente dome, extending 2.5 km by May 1987, 2.9 km by June, and entering the Río Nima II valley (Fig. 2). The TM image of 25 October 1987 showed that the flow had extended a further 700 m, giving an advance rate of ~5 m day^{-1} during June–October compared with ~13 m day^{-1} during May–June. This reduction in advance rate is consistent with Andres and Rose (1995) and SEAN (1988b) who mark the flow front in the same position during February 1988. This indicates that the ~3.6-km-long flow front stagnated around this time. The TM image of November 1988 reveals a new ~1.1-km-long block flow extending over the proximal section of the 1986–1987 flow (Fig. 2). By March 1989 this flow was 70 m wide and 20 m thick (SEAN 1989b) and had extended to 2.1 km giving an advance rate of ~7 m day^{-1} (Fig. 2).

Caliente IVb (1989–1996)

By January 1990, block flow activity to the south had ceased and extrusion was focused at the Caliente vent, with a short flow unit extending 0.9 km SE in January and 1.1 km SW in March (Fig. 3). During July 1990 a 2-km-long, 30–50-m-wide, 15–20-m-high block flow advanced down the east flank of the dome (BGVN 1990). Block flows ≤1.25 km long extending down the east and west flanks of the dome were apparent on all images acquired during 1991–1992, with the Río Nima I/II watershed causing flow toes to be deflected to the SW (Fig. 3). This
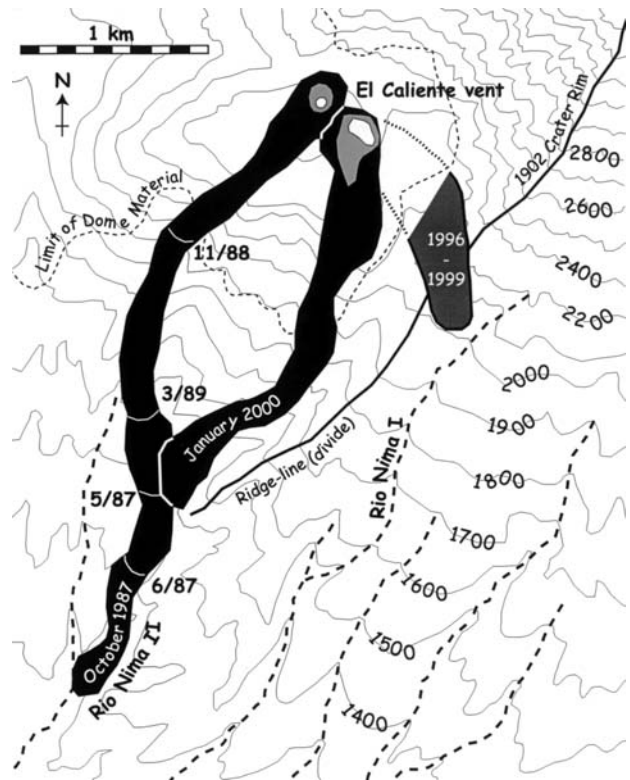
Fig. 2 Block flow units active during October 1987, 1996–1999, and January 2000 mapped using Landsat data: 1987 and 1989 flow fronts are taken from SEAN (1988a, 1988b, 1989b) and the 1988 flow front is placed using the November 1988 TM image. The proximal section of the 1996–1999 unit could not be traced on the Landsat images, or from aerial photographs, its margins (*dashed*) are therefore inferred. *Black*, *gray*, and *white tones* locate thermally anomalous surfaces in TM bands 6 (>55 °C), 7 (>120 °C), and 5 (>220 °C), respectively

is consistent with ground-based observations that describe the flow front as stagnated with lava piling up on the upper eastern flanks of the Caliente dome by November 1991 (BGVN 1991). A similar situation is assumed from the location of flow front collapse plumes in May 1992 (BGVN 1992). The TM images indicate that block flow activity had ceased by January 1993, when extrusion had become restricted to the vent region. However, by February, two block flow units were apparent extending ~0.6 km to the SE and SSE (Fig. 3). Field observations during November 1993 showed that these flows had extended 1 km, with additional 300- and 100-m-long lobes extending SW and E (BGVN 1993). By December, extrusion was restricted to the vent region once more (Fig. 3). Activity continued in this manner throughout 1994–1996 with periods of at-vent extrusion punctuated by block flow extension down the S and E dome flanks, with flows extending ≤1.25 km either to pond at the base of the Río Nima I/II watershed, or be deflected by it (Fig. 3).

Fig. 3 Location of active lava mapped using Landsat data during 1988–1996. Maps are fitted to a contour map of the Caliente dome. *Black*, *gray*, and *white tones* locate thermally anomalous surfaces in TM bands 6 (>55 °C), 7 (>120 °C), and 5 (>220 °C), respectively. The extents of larger units mapped using Landsat data and emplaced during 1987–1989, 1996–1999, and 1999–2000 are given in Fig. 2
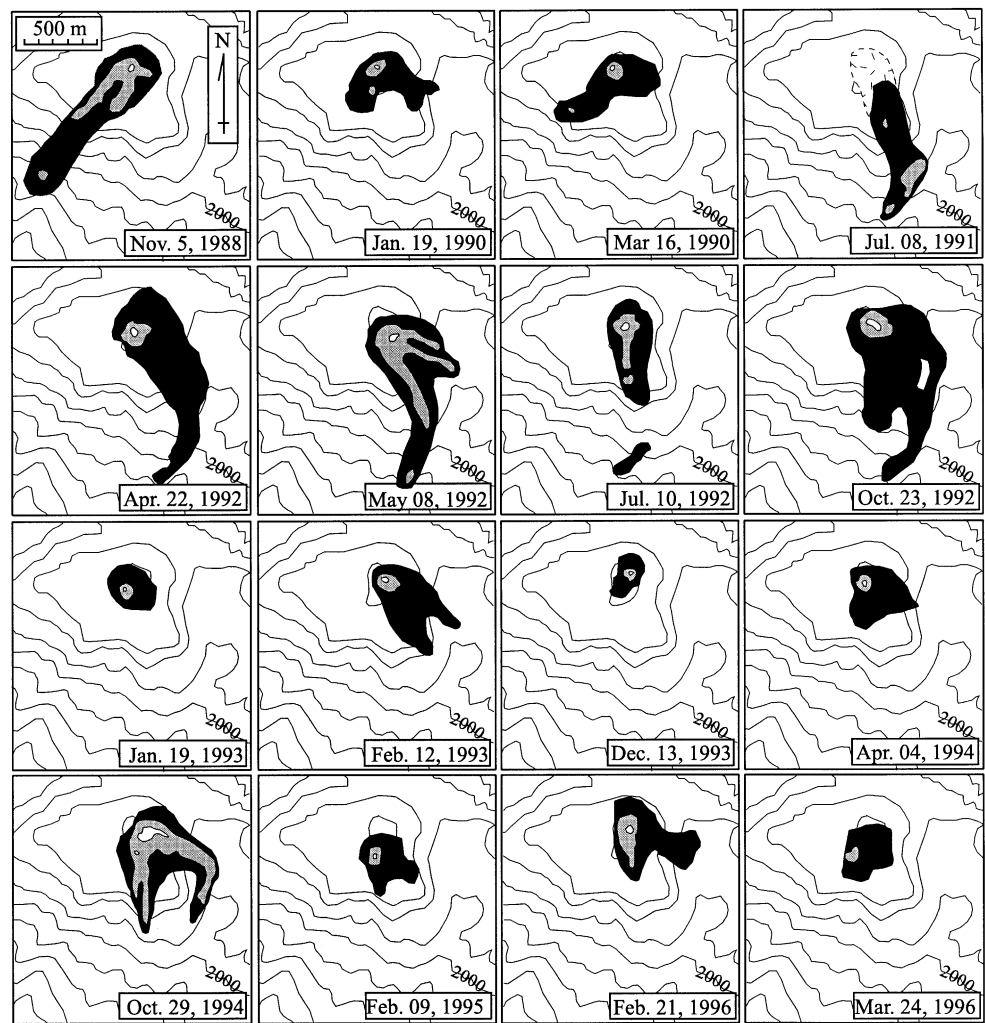
Caliente V (1996–2000)

Although reports indicate that a flow on the ESE flank of the Caliente overtopped the 1902 crater rim and extended into the headwaters of the Río Nima I during 1995 (BGVN 1999a), there is no sign of this flow on TM images obtained during 1995–1996. Unfortunately, due to the gap in the Landsat archive for Santiaguito during 1997–1999, we are unable to determine exactly when this flow was emplaced. However, by January 2000, the presence of a new, but inactive, flow is obvious in that location. This unit extended ~1.1 km to the SE, causing a ~400-m-wide breach in the 1902 crater rim and reaching the floor of the Nima I valley (Fig. 2). Reports of lava extrusion beginning in an easterly direction during March 1996, followed by continued extrusion and lahar activity in the Nima I during 1997–1998 (BGVN 1999a), indicate that this large block flow unit was emplaced at that time.

Breaching of the 1902 crater rim by the 1996–1999 flow was facilitated by continuous activity on the east flank of Caliente during 1990–1996, which caused the 1902 crater rim to be increasingly buried by a pile of talus and block flows. This is apparent from shadows on the TM images. These indicate that the height of the crater rim at its lowest point, SE of the Caliente vent where the 1996–1999 breach occurred, decreased from 90±18 m in 1987 to 27±9 m by February 1996.

By January 2000, a second large block flow had extended ~2.4 km down the Caliente S flank and into the headwaters of the Rio Nima II, having been deflected SW by the Nima I/II divide (Fig. 2). Field observations by us on 23 January 2000 showed that the proximal section of this flow was 60–100 m wide and ~40 m thick, and the flow front was ~200 m wide and 18–30 m high (Harris et al. 2002). Reports of dome extrusion, repeated pyroclastic flows, and south-moving flows in July 1999 (BGVN 1999b), along with an increase in hot spot activity observed using the GOES hot spot monitoring tool (http://goes.higp.hawaii.edu/) during mid-July, indicate that this flow began advancing at that time. This gives an advance rate of 12.5 m/day for this block flow unit.

Extrusion rates 1986–2000

Satellite-data-derived extrusion rates: method

Following Harris et al. (1998, 2000), we calculate extrusion rate (E_r) from:

$$E_r = Q_{tot}/[\rho(C_p\Delta T + c_L\Delta\phi]\tag{1}$$

where Q_{tot} is total thermal flux from the active lava unit, ρ and C_p are lava density and specific heat capacity, ΔT is lava cooling, c_L is the latent heat of crystallization, and $\Delta\phi$ is the mass fraction of magma that crystallizes in cooling through ΔT. We correct ρ (2,600 kg m^{-3}) and C_p (1,150 J kg^{-1} K^{-1}) for $\leq$30% vesicles (Anderson et al. 1995). We use $\Delta\phi$ of 0.45, calculated from Stoiber and Rose (1969), and set ΔT to ~330 °C, using an eruption temperature (T_{erupt}) of ~830 °C(Scaillet et al. 1998) and the maximum core temperature obtained by us at the flow front in January 2000 of ~500 °C.

Q_{tot} is the sum of heat loss by radiation (Q_{rad}) and convection (Q_{conv}) from the flow surface, plus conduction through the base (Q_{cond}), where

$$Q_{rad} = \sigma\varepsilon A_{lava}T_e^4\tag{2}$$

$$Q_{conv} = 0.14A_{lava}\kappa(g\alpha\rho/\mu\kappa)^{1/3}(T_e-T_{air})^{4/3}\tag{3}$$

$$Q_{cond} = A_{lava}\kappa_{lava}[(T_{erupt}-T_{base})/h_{base}]\tag{4}$$

A_{lava}, σ, ε, g and T_{air} being flow area, Stefan–Boltzmann's constant, lava emissivity (0.99), acceleration due to gravity, air temperature (~20 °C); k, μ, κ, α, and ρ are air thermal conductivity, dynamic viscosity, thermal diffusivity, cubic expansivity, and density (set using Kays and Crawford 1980); and κ_{lava} is lava thermal conductivity (calculated following Peck 1978). T_e is the effective radiation temperature of the flow surface and is given by

$$T_e = [pT_h^4+(1-p)T_c^4]^{0.25}\tag{5}$$

T_h and T_c being the crack and crust temperature at an active flow surface, and p is the surface portion occupied by cracks. T_{base} and h_{base} are the temperature and thickness of the basal thermal boundary layer, where we assume that $T_{base} \approx T_c$, and h_{base} approximates the thickness of the surface thermal boundary layer (h_{surf}) calculated following Oppenheimer (1991) from

$$h_{surf} = \kappa_{lava}A_{lava}(T_{erupt}-T_{base})/(Q_{rad}+Q_{conv})\tag{6}$$

From Eqs. (1), (2), (3), (4), (5), and (6) it is clear that a measure of the thermal structure of the flow surface is required to provide T_h, T_c, and p, as well as flow area (A_{lava}). Following Harris et al. (1999a, 1999b), we obtain these by adapting the dual-band approach first applied to obtain lava flow surface thermal structures from TM data by Rothery et al. (1988). In this case, T_h, T_c, p, and A_{lava} are obtained using emitted thermal radiation in TM bands 5 (1.55 –1.75 μm), 6 (10.42–12.42 μm), and 7 (2.08–2.

35 μm) in the solution of the following simultaneous equations:

$$R_5 = p_bL_5(T_b) + pL_5(T_h) + (1 - p_b-p)L_5(T_c)\tag{7a}$$

$$R_6 = p_bL_6(T_b) + pL_6(T_h) + (1 - p_b-p)L_6(T_c)\tag{7b}$$

$$R_7 = p_bL_7(T_b) + pL_7(T_h) + (1 - p_b-p)L_7(T_c)\tag{7c}$$

in which R_5, R_6, and R_7 are the at-satellite radiances corrected for atmospheric, surface emissivity and reflection effects, in bands 5, 6, and 7; L_λ is the Planck function for TM band λ (λ=5, 6, or 7); p_b is the pixel portion occupied by ambient ground surrounding the sub-pixel lava body; and T_b is the temperature of the ambient ground.

Because pixel areas are different between bands 5, 6, and 7 (being 900 m^2 in bands 5 and 7, and 14,400 or 3,600 m^2 for TM or ETM+ band 6, respectively) we must ensure that the three radiances used in Eq. (7) relate to the same surface area. To do this we assume that the area of thermally anomalous band 6 pixels contains the entire active lava area, and calculate an integrated radiance in band λ ($R_{\lambda int}$) from

$$R_{\lambda int} = \sum_{i=1}^{n\lambda}\left(\frac{pixel_\lambda}{anom_6}R_\lambda i\right)\tag{8}$$

in which n_λ is the number of thermally anomalous pixels in band λ, $pixel_\lambda$ is the pixel area in band λ, $anom_6$ is the anomaly area in band 6, and $R_{\lambda i}$ is the emitted radiance in band λ for pixel i. Using R_{5int}, R_{6int} and R_{7int} in place of R_5, R_6, and R_7 in Eqs. (7a, 7b, and 7c), we arrange Eq. (7b) so that

$$\beta_6 = \{R_{6int}-L_6(T_c) - p[L_6(T_h)$$
$$-L_6(T_c)]\}/\{L_6(T_b) - L_6(T_c)\}\tag{9}$$

Substituting p_b in Eqs. (7a) and (7c) with β_6 now reduces the number unknowns to four (T_b, T_h, T_c, and p). T_b can be estimated using typical temperatures from background band 6 pixels surrounding the active flow and we set T_h equal to T_{erupt}. Assuming these values and using Eqs. (7a), (7c), and (9) therefore allows T_c and p to be calculated (Appendix). Solution enables A_{lava} to be estimated by multiplying the $1-p_b$ by $anom_6$.

Saturated pixels were rare. In fact 9 of the 18 images used had no saturated pixels, a result of the extensive, thick, cool crusts that characterize the surface of Santiaguito's block flows (Harris et al. 2002). Of the remaining images, just 1–20% of the pixels used were saturated. In these cases, the saturated value was used in Eq. (8) so that the result gave the minimum expected $R_{\lambda int}$.

This three-band-integrated-anomaly approach has three advantages over previous adaptations of the dual-band method. First, by integrating radiances over the entire anomaly area, the approach avoids error due to pixel mis-registration encountered when using pixel-by-pixel solutions. However, problems due to bleeding of radiance into surrounding pixels and pixel overlap remain. This could result in an over-estimate of the

summed radiance. Second, it allows lava area to be estimated without pixel counting, where the inclusion of partially full pixels or pixels containing radiance due to bleeding by the pixel counting approach are know to result in large over-estimates of A_{lava} (Harris et al. 1999a). Third, only two assumptions (T_b and T_h) are required, where these are parameters on which tightest constraint is possible using image-derived background surface temperatures and eruption temperatures, respectively. Our remaining unknowns that we obtain from solution of our approach, T_c, p, and p_b, are notoriously variable and impossible to assume with any degree of certainty.

Wright et al. (2001) show that, in cases where only one or two bands of data are available (so that T_c is assumed to solve for lava area), E_r becomes a function simply of lava area (i.e., $E_r = m\ A_{lava}$). Indeed, inspection of in Eqs. (1), (2), (3), and (4) shows that in such cases A_{lava} becomes the only variable. Our new approach, however, also allows T_c to be calculated so that E_r is a function of flow area and surface temperature, and hence heat loss. In the case of Wright et al. (2001), it is argued that the term m that relates E_r and A_{lava} can be viewed as an empirically parameterized constant, which provides an approximation of E_r "in a manner that is both qualitatively and quantitatively consistent with ground based data". Here comparisons with ground-based data (included in the discussion that follows) show an equally good agreement with satellite-derived E_r when E_r is set in as a function of both A_{lava} and T_c (or Q_{tot}).

Calculated thermal structure and lava area

Calculated crust temperatures fall in the range 90–255 °C, with a mean and standard deviation of 164 and 64 °C(Fig. 4). This compares well with field measurements, where we made 121 crust temperature measurements at the front of the active block flow on Santiaguito during 23 January 2000. These measurements gave a T_c range of 29–303 °C, with a mean and standard deviation of 120 and 67 °C. Derived flow area also shows good agreement with those occasions when field-based flow dimension estimates allow comparison (Fig. 5). The percentage of the surface occupied by cracks was low in all cases (Fig. 5) and all calculated values for p were <0.25% with a mean and standard deviation of 0.05 and 0.06%. This is to be expected at slow moving, heavily crusted block flows.

Extrusion rates and volume

Application of the above methodology allow extrusion rates during 1988–2000 to be estimated. Using these results, we estimate the volume of emplaced material by integrating our extrusion rates through time. Being based on a measure of the extrusion rate, such volume estimates are not subject to the error resulting from missing, eroded volume that affects estimates obtained using post-em-
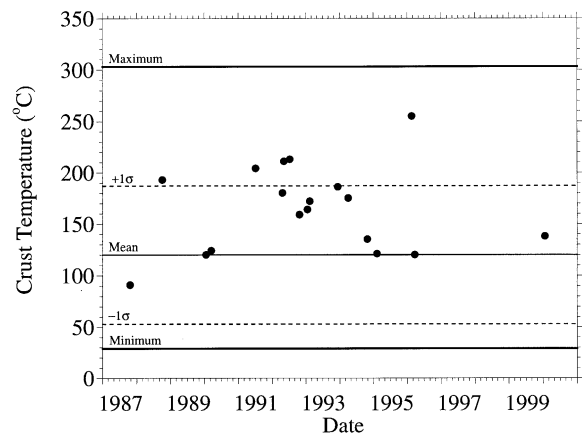
Fig. 4 Landsat-derived crust temperatures (*solid circles*) with mean, standard deviation and range of field measurements (*horizontal lines*) made in January 2000
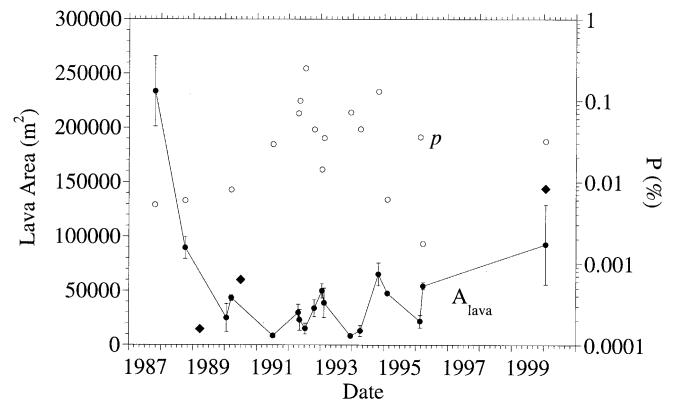
Fig. 5 Landsat-derived lava area (*solid circles*) and surface percentage occupied by high temperature cracks (*open circles*), with lava areas estimated from ground-based dimensions (*solid diamonds*)

placement dome unit dimensions. Using the Landsat data, we are thus able to estimate extrusion rates during the 7th cycle of extrusion at Santiaguito, and the beginning of the 8th cycle (Fig. 6).

Caliente IVa (1986–1989)

As already discussed, ground reports indicate that the 7th cycle of extrusion began at the Caliente vent during June 1986 (SEAN 1988b). Highest extrusion rates obtained during TM acquisitions were coincident with the emplacement of the two long block flow units, during which extrusion rates of 0.72±0.08 and 0.84±0.11 m³ s⁻¹ were obtained on 25 October 1987 and 5 October 1988, respectively (Fig. 6). These compare with rates of 0.35–0.90 m³ s⁻¹ obtained using an advance rate of 5–13 m day⁻¹, flow thickness of 30 m estimated from ground-based reports during May–October 1987 (SEAN 1988a), and a width of ~200 m obtained from the TM
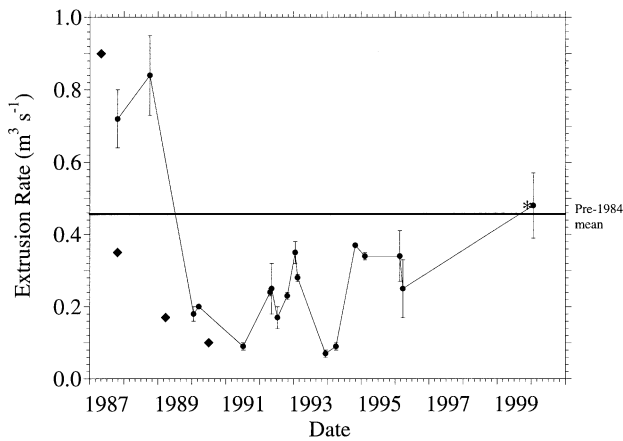
Fig. 6 Landsat-derived extrusion rates (*solid circles*), with extrusion rates estimated from ground-based flow dimensions and advance rates obtained during cycles 7 (1986–1996) and 8 (1996–ongoing). *Solid diamonds* indicate extrusion rates calculated from ground reports and *TM data* and * are calculated using our own field measurements

image. Field-based flow dimensions (width =70 m, thickness =20 m) obtained during March 1989 (SEAN 1989b), along with an advance rate (7.2 m day^{-1}) obtained using the difference between November 1989 TM recorded length and the March 1989 field-based length, indicate extrusion rates of ~0.12 m^3 s^{-1} at that time. This lower extrusion rate may indicate the end of this high extrusion rate phase during 1989, with the phase lasting ~3.6 years and adding 0.07 km^3 of lava to Santiaguito mostly in the form of long block flow units extending beyond the flanks of the Caliente dome.

Caliente IVb (1989–1996)

Ground (BGVN 1990) and TM-derived extrusion rates show lower (0.07–0.37 m^3 s^{-1}) extrusion rates persisting throughout 1990–1995 (Fig. 6). Therefore, we identify the low extrusion rate phase of cycle 7 as lasting 6.2 years until March 1996 when the first large flow that breached the 1902 crater rim was reported (BGVN 1999a). During this low extrusion rate phase, a further 0.04 km^3 of lava

was added to Santiaguito by the emplacement of short block flows on the dome flanks and extrusion of dome material within the Caliente vent zone. Extrusion rates were highest (0.17–0.37 m^3 s^{-1}) during the block flow emplacement events of 1992–1993 and 1994–1996, and lowest (0.07–0.20 m^3 s^{-1}) during the intra-vent extrusion of 1990 and 1993–1994 (Fig. 6).

Caliente V (1996–2000)

By January 2000, TM-calculated extrusion rates had increased to 0.48±0.09 m^3 s^{-1} (Fig. 6), consistent with our ground-based estimate of 0.48±0.17 m^3 s^{-1} based on a flow width of 60–100 m, a depth of 40 m, and a time-averaged velocity of 12.5±1.5 m day^{-1}. This increase to above the pre-1984 time averaged extrusion rate marked the onset of the 8th cycle of extrusion. We assume that this cycle began with the extension of the 1902 crater rim breaching flows in March 1996. By January 2000, extrusion during this cycle had added 0.06 km^3 of lava to Santiaguito. This lava was emplaced mostly as two large block flows to the SE and S (Fig. 1).

Discussion

The chronologies detailed above reveal a number of trends including (1) a transition from endogenous to exogenous growth, (2) a migration of vent location first in a westward direction, and then back to the original vent location, and (3) a decline in extrusion rates. We next attempt to explain each of these trends.

Transition from endogenous and exogenous growth

Since 1922, the style of extrusion has evolved from endogenous- to exogenous-(block lava flow) dominated emplacement (Table 1; Rose 1987). Block flows were first emplaced during at the end of cycle 1 (1925–1929), to become increasingly dominant from cycle 4 (1949–1958) onwards. Cycles 6–8 (1972–2000) were then dominated by block flow emplacement. Two existing

Table 1 Characteristics of each cycle of extrusion at Santiaguito 1922–2000. E_r Extrusion rate; L_{max} Maximum block lava flow length

Cycle	Location	Duration (years)		Character	E_r (m^3 s^{-1})		L_{max} (km)
		High	Low		Mean	Max.	
1 (1922–1929)	Caliente I	3	4	Endogenous	0.9	2.1	
2 (1929–1939)	Caliente II	5	5	Transitional		0.6	0.7
3 (1939–1949)	La Mitad	3	7	Transitional		0.9	
4 (1949–1958)	El Monje	6	3	Transitional	0.7	1.2	1.0
5 (1958–1972)	El Brujo	5	9	Exogenous	0.5	1.5	2.3
6 (1972–1986)	Brujo/Caliente III	3	11	Exogenous	0.5	0.9	2.1
7 (1986–1996)	Caliente IV	4	7	Exogenous	0.3	0.8	3.6
8 (1996–[a])	Caliente V	[a]		Exogenous		0.5	3.6[b]

[a] High extrusion rate cycle is on-going as of January 2002
[b] Still advancing as of January 2002

dome growth models can be used to explain this transition.

First, following Blake (1990), the transition from a lava dome to block flow depends on the relationship between the underlying slope (θ) and yield strength (τ). Flow in a preferential direction will develop if

$$h_o/\sin(\theta) < (h_o R)^{1/2} \qquad (11)$$

where R is the dome radius and h_o is the characteristic length scale. Following Blake (1990)

$$h_o = \tau \rho g \qquad (12)$$

in which ρ and g are lava density and acceleration due to gravity, and

$$\tau = (0.0323 \pm 0.0016)(H^2 \rho g / R) \qquad (13)$$

where H is dome height.

Second, following Fink et al (1990), Denlinger (1990), and Iversen (1990), exogenous growth will occur if magma pressure within the dome exceeds the tensile strength of the containing shell across which slow crack growth is occurring. Denlinger (1990) thus relates time to rupture (t_f), pressurization, and slow crack growth using:

$$t_f = \underbrace{\frac{2}{n-2}}_{1} \underbrace{\left[\frac{K_{Ic}^2}{Y^2 \sigma_c^2 v_c^2}\right]}_{2} \underbrace{\left(\frac{\sigma_a}{\sigma_c}\right)^{-n}}_{3} \underbrace{\left[\ln\left(\frac{1}{1-P}\right)\right]^{(n-2)/m}}_{4} \qquad (14)$$

Term : 1   2   3   4

in which n and m are constants, and K_{Ic}, Y, σ_c, v, σ_a, and P are stress intensity factor for tensile loading at rupture, a dimensionless geometric factor, stress at which the shell ruptures immediately, crack velocity at rupture, applied stress due to dome overpressure, and probability of failure (10^{-6} to 1), respectively. Following Denlinger (1990), we set term 2 equal to 25 s and use $\sigma_a = H \gamma$, with γ being unit pressure (26,000 Pa). Following Eq. (14), increased dome thickness will decrease t_f, where writing A, B, and D for terms 1, 2, and 4 and re-arranging allows critical thickness for failure (H_{crit}) at time t_f to be calculated from

$$H_{crit} = \frac{\sigma_c \left(\frac{t_f}{ABD}\right)^{-(1/n)}}{\gamma} \qquad (15)$$

By 1925, the eruption of Santiaguito had been underway for 3 years and the dome volume had reached 0.2 km^3. We use a dome diameter (D) of ~1,000 m and, for simplicity, assume a disc-shaped dome to obtain H from $V/\pi r^2$, V and r being dome volume and radius, respectively, giving H of 255 m. This compares with H of ~250 m estimated from photographs taken in 1925. Given the 1925 dimensions and assuming emplacement on a relatively flat crater floor ($\theta = 1-5°$), we obtain τ of 0.1 MPa and find that conditions favor dome growth, i.e., the right-hand term in Eq. (11) is greater than the left-hand term. Rheology prior to 1925, therefore, did not favor formation of block lava flows.

However, by 1925, pressurization parameters did favor formation of block lava flows by failure of the outer carapace. In this regard, the 1925 dome height of ~250 m produces an overpressure such that Eq. (14) indicates immediate failure of the outer shell, thus allowing exogenous extrusion. Given t_f of 3 years then H_{crit} is ~36 m. This is well below the expected H for 1925. The conflicting results of the rheological and pressurization model for 1925 appear consistent with the onset of a transitional stage of activity at the time during which both endogenous dome growth and block flow emplacement occurred (Table 1).

By 1958, however, both the rheological and pressurization parameters favored block flow. This may explain the end of the transitional stage and the onset of a block-flow-dominated activity. Given the 1958 dome volume (0.5 km^3) and diameter (2,000 m), with calculated H and τ of 160 m and 0.02 MPa, Eq. (11) indicates that rheological conditions favored flow. Thus, while pressurization favors extrusion due to carapace failure by 1925, rheological factors do not favor flow until 1958. Thus, as observed (Table 1), an increasing dominance of flow over dome unit emplacement should be expected between 1925 and 1958 as pressurization and rheological factors become increasingly conducive to first carapace failure and then non-radial spreading.

Volumetric trends during the 1922–2000 Santiaguito eruption

Sustained lava extrusion at a time-averaged rate of 0.44±0.01 m^3 s^{-1} during 1922–2000 built a ~1.1-km^3 dome complex at Santiaguito. Given the possible under-estimate in pre-1980 dimension-based volumes due to post-emplacement erosion, the total dome volume emplaced may be as high as 1.3 km^3, yielding a maximum time-averaged extrusion rate of 0.53±0.01 m^3 s^{-1}. We note that this volume is only ~10% of the mass erupted during the 1902 eruption, and that this whole body is substantially degassed.

Extrusion at Santiaguito has been cyclic, alternating between periods of high and low extrusion rates (Fig. 7a). In Fig. 7b we have plotted these data as cumulative volume and time-averaged extrusion rate. We define time-averaged extrusion rate by dividing the total volume erupted at any point in time (cumulative volume) by the time since the eruption began. Figure 7b shows that the time-averaged extrusion rate has decayed exponentially, with the high extrusion rate phases of each subsequent cycle causing slight irregularities in this trend.

Data gathered here also allow us to detail the extrusion rates, and calculate the time-averaged extrusion rate and cumulative volume during a single cycle (Fig. 8). These single cycle data show a similar trend. The total volume of cycle 7 was 0.12 km^3, giving a time-averaged eruption rate for this 9.8-year-long cycle of 0.38 m^3 s^{-1}. Of this total volume, 64% was extruded during the first 3.6 years (37% of the cycle by duration). This is apparent from the extrusion rates, which show an exponential decay from 0.72–0.90 m^3 s^{-1} during the high extrusion rate phase to 0.07–0.37 m^3 s^{-1} in the low phase, and the time-averaged
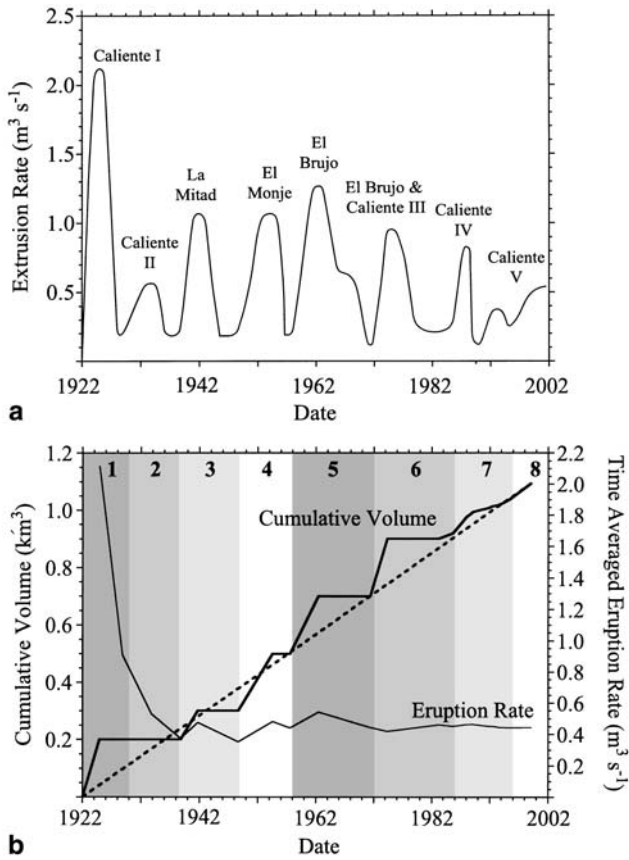
Fig. 7 a Estimated variation in extrusion rate at Santiaguito since 1922 showing the eight main extrusion cycles during the period 1922–2000. This plot is an up-dated version of that given by Rose (1987) for the period 1922–1980. **b** Cumulative volume (*thick solid line*), eruption rate (*thin solid line*), and cumulative volume given steady extrusion at the 1922–2000 time-averaged rate of 0.44±0.01 m³ s⁻¹ (*thick, dashed line*). Here, eruption rate is the cumulative volume divided by time since the beginning of the eruption (1922). Cycles are identified by *numbered gray zones*
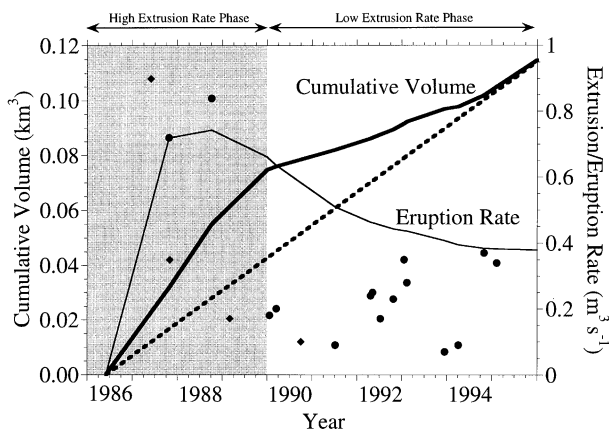
Fig. 8 Cumulative volume (*thick solid line*), eruption rate (*thin solid line*), individual extrusion rates (Landsat-based = *solid circles*; ground-based = *solid diamonds*) and cumulative volume given steady extrusion during this cycle at the 1986–1995 time-averaged rate of 0.38 m³ s⁻¹ (*thick, dashed line*). In this case, eruption rate is the cumulative volume divided by time since the beginning of the cycle (1986). High and low extrusion rate phases of the cycle are identified by *gray and white zones*
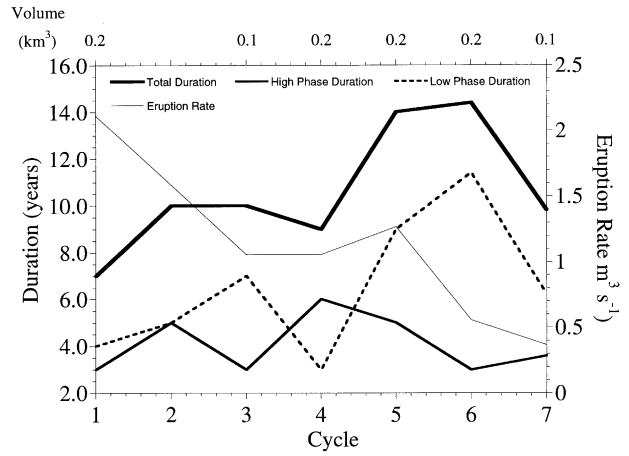
Fig. 9 Cycle, high and low phase durations, with cycle eruption rate (cycle volume divided by cycle duration). Lava volume emplaced during each cycle is given along the top of the graph

extrusion rate, which shows a rapid increase followed by a steady decline (Fig. 8).

The time-averaged extrusion rate during each cycle (cycle volume divided by cycle duration) and cycle duration are summarized in Table 1 and Fig. 9. These data indicate that the time averaged eruption rate for each cycle has also declined through time. At the same time, the total cycle duration has increased. This is due mostly to an increase in the duration of the low extrusion rate phase during each cycle, i.e., the repose between high extrusion rate phases has increased with time (Fig. 9). There is also evidence that maximum extrusion rates during each cycle have been declining (Fig. 7a). This has been especially true of cycles since 1958 (Table 1). We next consider the possible implication of these trends in terms of vent location and system pressurization.

Declining extrusion rates: the cause of a shift in vent location?

The eastward shift in eruption center between 1972 and 2000 could be a symptom of gradual decline in extrusion rates. Prior to 1972, activity had moved progressively westwards, away from the central conduit below the 1902 vent. However, the dual-location activity that occurred during cycle 6 (1972–1986) marked a significant shift in the location of activity back to the region of the 1902 vent. This likely reflects a decrease in driving pressure (dp/dx) in the shallow conduit system that fed the west-lateral vents, where

$$E_r = -\frac{\pi r^4}{8\mu}\frac{dp}{dx} \qquad (17)$$

in which r is conduit radius and μ is the fluid viscosity. Given a decrease in E_r from 1.5 m³ s⁻¹ in 1958 to 0.5 m³ s⁻¹ by 2000, then dp/dx would have declined by 33%, causing the western, distal portions of the shallow conduit system

to gradually shut down. A similar effect was observed at Kilauea by Kauahikaua et al. (1996). In this case, a gradual decline in effusion from the distal section of the dyke that fed the Pu'u 'O'o-Kupaianaha eruption was ascribed to a decrease in driving pressure. This eventually caused the distal Kupaianaha vent to shut down and the eruption to establish up-rift at the Pu'u 'O'o vent.

Eruption from a pressurized source?

The exponential decay in time-averaged eruption rate (Fig. 7b) is similar to trends observed during pressurized, basaltic, effusive eruptions. These basaltic cases have typically been observed to evolve over periods of days to months, with eruption rate peaks of tens to thousands of cubic meters per second (Wadge 1981; Harris et al. 2000). In the dacitic case considered here, the trend appears to have evolved over a period of decades and peak extrusion rates are <5 m^3 s^{-1}. According to such a model, the opening of a conduit linking a pressurized source to the effusive vent would generate the initial high extrusion rate peak. Continued supply of magma to the open conduit would then supply the depressurized, lower extrusion rate period. A similar pressurized trend is apparent during cycle 7 (Fig. 8), where periods of increased supply will cause similar, shorter (year-long) trends to be superimposed on the longer term trend as the conduit becomes pressurized and depressurized during the course of each cycle.

The depressurization model is consistent with increased low extrusion rate phase duration and decreased time averaged (and peak) eruption rates during each cycle (Fig. 9). This would be expected during steady exhaustion and continued depressurization of the source. If this trend continues, with the time-averaged eruption rate declining at a rate of -0.25 m^3 s^{-1} per cycle, then the 9th cycle should be the last. Given the 9–14-year-long duration of cycles 6 and 7, then this places a termination to the current extrusive activity around 2014–2024.

Anderson et al. (1995) argue an alternative model, suggesting that the Santiaguito dome attained a critical size and strength in 1925, impeding extrusion, reducing extrusion rates, and allowing more thorough degassing to take place leading to denser, smooth textured erupted products. Our model also allows for increasingly degassed lavas, but in our case lower extrusion rates to allow more thorough degassing are instead explained by depressurization.

There is, however, also a trend for extrusion rates during high extrusion rate phases to approach those of the low phases. This, along with the approximately linear increase in cumulative volume and leveling-off of the eruption-rate curve since ~1939 (Fig. 7b), may indicate that a steady, persistent supply regime is becoming established. In this case, the current cyclic extrusion mode may become increasingly replaced by less cyclic, persistent extrusion at lower (0.2–0.4 m^3 s^{-1}) rates.
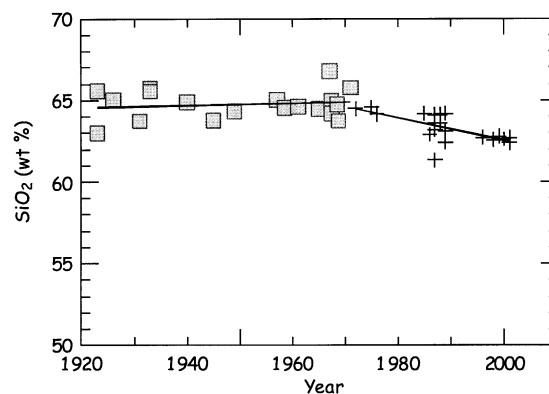
Fig. 10 Temporal variation in SiO_2 of erupted lavas at Santiaguito 1922–2001. *Gray squares* signify lavas erupted prior to 1970 and *crosses* signify post-1970 lavas

Additional evidence from compositional changes and block lava flow length

An analysis of 39 lava samples erupted from Santiaguito between 1922 and 2001 indicate a steady decline in SiO_2 weight fractions (X_{SiO2}) since ~1970, with a decrease from ~65 to ~63 wt% (Fig. 10). Following Bottinga and Weill (1972), log viscosity (η) correlates almost linearly with X_{SiO2} [$\eta=0.0004\exp^{0.1737XSiO2}$, correlation coefficient =0.95], so that the above decrease in X_{SiO2} would result in a ~30% decrease in viscosity.

From Table 1, we also note a steady increase in the length attained by block lava flows erupted during each cycle, in-spite of declining extrusion rates. The trend is especially apparent in block flow lengths since 1958. This trend could be symptomatic of the decreasing silica content and, thus, viscosity of the erupted lavas during the same period.

A similar compositional trend was noted at Mount St. Helens during May–December 1980, with the erupted magma generally becoming more mafic with time (Lipman et al. 1981). Lipman et al. (1981) interpreted these changes as representing samples from successively deeper levels in a compositionally zoned or stratified magma body. When considered with the exponential decay in extrusion rates such a model may be consistent with the Santiaguito case. This leads us to favor a model whereby tapping of an increasingly exhausted chamber has resulted in declining extrusion rates (both time averaged and peak), an increase in the duration of low extrusion rate phases, and a decrease in SiO_2 content as deeper, more mafic magmas are erupted.

Conclusions

Our satellite-based method of extracting extrusion rates represents a reliable means of adding to extrusion-rate datasets more commonly obtained from volumetric changes estimated using theodolites, laser distance meters, GPS, and aerial photographs (e.g., Sparks et al 1998;

Nakada et al. 1999). For Santiaguito, application of this methodology has allowed constraint of extrusion rates typical of the eruption cycles that have been continuing since the current eruption began in 1922.

For Santiaguito, an analysis of the extrusion rate data allow a number of observed changes in the location and style of activity to be assessed in terms of physical processes.

1. A progressive transition from endogenous to endogenous growth during 1925–1958 may be explained by changing pressurization and rheological conditions. The onset of endogenous activity in 1925 may be explained by dome over-pressurization causing failure of the outer carapace, allowing exogenous units to leak out. Thereafter, increasingly favorable rheological conditions may explain the dominance of block lava flow activity after 1958.
2. Declining extrusion rates correlate with the cessation of activity at lateral vents, such that activity has become focused above the main conduit. Waning activity at distal sections of the system may be a symptom of reduced driving pressure brought about by declining extrusion rates.
3. Declining time averaged extrusion rates, coupled with a decrease in peak extrusion rates during high extrusion rate spurts and an increase in the duration of low extrusion rate periods, may indicate steady depressurization of the source.
4. When considered with a steady decrease in SiO_2 content, the decaying extrusion rate trend appears to be consistent with progressive chamber exhaustion. Decreased lava viscosity also resulting from the change in SiO_2 content can also explain an increase in block lava flow length.

In this case, eruption of magma from deeper, mafic levels in an increasingly exhausted and depressurized chamber explain the gradual transition to the current stage of mafic lavas erupted at a declining rate. If these mafic lavas do represent deeper chamber zones, then this may be evidence that the current eruption at Santiaguito is coming to an end. The emplacement of increasingly extensive block lava flows and vent relocation may be a symptom of this demise.

Appendix

We solve Eqs. (7a) and (7b) using:

$$p_h7 = \{C_7 - [C_6A_7]/A_6\}/\{B_7 - \{(B_6/A_6)A_7]\}$$

$$p_h5 = \{C_5 - [C_6A_5]/A_6\}/\{B_5 - \{(B_6/A_6)A_5]\}$$

in which p_{h7} and p_{h5} are p_h calculated in bands 7 and 5, and where for band λ,

$$A_\lambda = L_\lambda(T_b) - L_\lambda(T_c)$$

$$B_\lambda = L_\lambda(T_h) - L_\lambda(T_c)$$

$$C_\lambda = R_{\lambda int} - L_\lambda(T_c)$$

We then solve by iteration, varying T_c until $p_{h7} = p_{h5}$.

References

Anderson SE, Fink JH, Rose WI (1995) Mount St. Helens and Santiaguito lava domes: the effect of short-term eruption rate on surface texture and degassing processes. J Volcanol Geotherm Res 69:105–116

Andres RJ, Rose WI (1995) Description of thermal anomalies on two active Guatemalan volcanoes using Landsat Thematic Mapper imagery. Photogram Eng Remote Sensing 61:775–782

BGVN (1990) Santa Maria. Smithsonian Inst Bull Global Volcanism Network 15(11)

BGVN (1991) Santa Maria. Smithsonian Inst Bull Global Volcanism Network 16(11)

BGVN (1992) Santa Maria. Smithsonian Inst Bull Global Volcanism Network 17(5)

BGVN (1993) Santa Maria. Smithsonian Inst Bull Global Volcanism Network 18(11)

BGVN (1999a) Santa Maria. Smithsonian Inst Bull Global Volcanism Network 24(3)

BGVN (1999b) Santa Maria. Smithsonian Inst Bull Global Volcanism Network 24(12)

Blake S (1990) Viscoplastic models of lava domes. In: Fink J (ed) Lava flows and domes. Springer, Berlin Heidelberg New York, pp 88–126

Bottinga Y, Weill DF (1972) The viscosity of magmatic silicate liquids: a model for calculation. Am J Sci 272:438–475

Denlinger RP (1990) A model for dome eruptions at Mount St. Helens, Washington based on subcritical crack growth. In Fink J (ed) Lava flows and domes. Springer, Berlin Heidelberg New York, pp 70–87

Fink JH, Malin MC, Anderson SW (1990) Intrusive and extrusive growth of the Mount St. Helens lava dome. Nature 248:435–437

Flynn LP, Mouginis-Mark PJ, Horton KA (1994) Distribution of thermal areas on an active lava flow field: Landsat observations of Kilauea, Hawaii, July 1991. Bull Volcanol 56:284–296

Harris AJL, Flynn LP, Keszthelyi L, Mouginis-Mark PJ, Rowland SK Resing JA (1998) Calculation of lava effusion rates from Landsat TM data. Bull Volcanol 60:52–71

Harris AJL, Flynn LP, Rothery DA, Oppenheimer C, Sherman SB (1999a) Mass flux measurements at active lava lakes: implications for magma recycling. J Geophys Res 104:7117–7136

Harris AJL, Wright R, Flynn L (1999b) Remote monitoring of Mount Erebus Volcano, Antarctica, using polar orbiters: progress and prospects. Int J Remote Sensing 20:3051–3071

Harris AJL, Murray JB, Aries SE, Davies MA, Flynn LP, Wooster MJ, Wright R, Rothery DA (2000) Effusion rate trends at Etna and Krafla and their implications for eruptive mechanisms. J Volcanol Geotherm Res 102:237–269

Harris AJL, Vallance JW, Kimberly PG, Rose WI, Matias O, Flynn LP, Garbeil H (2001) Downstream aggradation owing to lava dome extrusion and rainfall runoff at Volcán Santiaguito, Guatemala. Geol Soc Am Bull (in press)

Harris AJL, Flynn LP, Matías O, Rose WI (2002) The thermal stealth flows of Santiaguito: implications for the cooling and emplacement of dacitic block lava flows. Geol Soc Am Bull 114(5):533–546

Iversen RM (1990) Lava domes modeled as brittle shells that enclose pressurized magma, with application to Mount St.

Helens. In: Fink J (ed) Lava flows and domes. Springer, Berlin, Heidelberg New York, pp 48–69

Kauahikaua J, Mangan M, Heliker C, Mattox T (1996) A quantitative look at the demise of a basaltic vent: the death of Kupaianaha, Kilauea Volcano, Hawai'i. Bull Volcanol 57:641–648

Kays WM, Crawford ME (1980) Convective heat and mass transfer. McGraw-Hill, New York

Kuenzi WD, Horst OH, McGehee RV (1979) Effect of volcanic activity on fluvial-deltaic sedimentation in a modern arc-trench gap, southwestern Guatemala. Geol Soc Am Bull 90:827–838

Lipman PW, Norton DR, Taggart JE, Brandt EL, Engleman EE (1981) Compositional variations in the 1980 magmatic deposits. In: Lipman PW, Mullineaux DR (eds) The 1980 eruptions of Mount St. Helens, Washington. US Geophys Soc Prof Pap 1250:631–640

Nakada S, Shimizu H, Ohta K (1999) Overview of the 1990–1995 eruption at Unzen Volcano. J Volcanol Geotherm Res 89:1–22

Oppenheimer C (1991) Lava flow cooling estimated from Landsat Thematic Mapper infrared data: the Lonquimay eruption (Chile 1989). J Geophys Res 96:21865–21878

Peck DL (1978) Cooling and vesiculation of Alae Lava Lake, Hawaii, US Geophys Soc Prof Pap 935-B

Rose WI (1972a) Notes on the 1902 eruption of Santa Maria Volcano, Guatemala. Bull Volcanol 36:29–45

Rose WI (1972b) Pattern and mechanism of volcanic activity at the Santiaguito volcanic dome, Guatemala. Bull Volcanol 36:73–94

Rose (1987) Volcanic activity at Santiaguito Volcano 1976–1984. Geol Soc Am 212:17–27

Rose WI, Stoiber RE, Bonis SB (1970) Volcanic activity at Santiaguito Volcano, Guatemala June 1968–August 1969. Bull Volcanol 34:295–307

Rose WI. Pearson T, Bonis S (1977) Nuée Ardente eruption from the foot of a dacite lava flow, Santiaguito Volcano, Guatemala. Bull Volcanol 40:23–38

SEAN (1986) Santa Maria. Smithsonian Inst Scientific Event Alert Network 11(11)

SEAN (1988a) Santa Maria. Smithsonian Inst Scientific Event Alert Network 13(2)

SEAN (1988b) Santa Maria. Smithsonian Inst Scientific Event Alert Network 13(11)

SEAN (1989a) Santa Maria. Smithsonian Inst Scientific Event Alert Network 14(7)

SEAN (1989b) Santa Maria. Smithsonian Inst Scientific Event Alert Network 14(6)

Rothery DA, Francis PW, Wood CA (1988) Volcano monitoring using short wavelength infrared data from satellites. J Geophys Res 93:7993–8008

Scaillet B, Clemente B, Evans BW, Pichavant M (1998) Redox control of sulfur degassing in silicic magmas. J Geophys Res 103:23937–23949

Simkin T, Sibert L (1994) Volcanoes of the world. Geoscience Press, Tucson

Sparks RSJ, Young SR, Barclay J, Calder ES, Cole P, Darroux B, Davies MA, Druitt TH, Harford C, Herd R, James M, Lejeune AM, Loughlin S, Norton G, Skerrit G, Stasiuk MV, Stevens NS, Toothill J, Wadge G, Watts R (1998) Magma production and growth of the lava dome of the Soufriere Hills Volcano, Montserrat, West Indies: November 1995 to December 1997. Geophys Res Lett 25:3421–3424

Stoiber RE, Rose WI (1969) Recent volcanic and fumarolic activity at Santiaguito Volcano, Guatemala. Bull Volcanol 33:475–502

Wadge G (1981) The variation of magma discharge during basaltic eruptions. J Volcanol Geotherm Res 11:139–168

Williams SN, Self S (1983) The October 1902 Plinian eruption of Santa Maria Volcano, Guatemala. J Volcanol Geotherm Res 16:33–56

Wooster MJ, Kaneko T, Nakada S, Shimizu, H (2000) Discrimination of lava dome activity styles using satellite-derived thermal structures. J Volcanol Geotherm Res 102:97–118

Wright W, Blake S, Harris AJL, Rothery DA (2001) A simple explanation for the space-based calculation of lava eruption rates. Earth Sci Planet Res Lett 192:223–233